Journal of Virology

Virology | Full-Length Text

Astrovirus replication is dependent on induction of double-membrane vesicles through a PI3K-dependent, LC3-independent pathway

Theresa Bub,[1,2] Virginia Hargest,[1] Shaoyuan Tan,[1] Maria Smith,[1,3] Ana Vazquez-Pagan,[1,3] Tim Flerlage,[1] Pamela Brigleb,[1] Victoria Meliopoulos,[1] Brett Lindenbach,[4,5] Harish N. Ramanathan,[4,5] Valerie Cortez,[6] Jeremy Chase Crawford,[7] Stacey Schultz-Cherry[1]

AUTHOR AFFILIATIONS See affiliation list on p. 15.

ABSTRACT Human astrovirus is a positive-sense, single-stranded RNA virus. Astrovirus infection causes gastrointestinal symptoms and can lead to encephalitis in immunocompromised patients. Positive-strand RNA viruses typically utilize host intracellular membranes to form replication organelles, which are potential antiviral targets. Many of these replication organelles are double-membrane vesicles (DMVs). Here, we show that astrovirus infection leads to an increase in DMV formation through a replication-dependent mechanism that requires some early components of the autophagy machinery. Results indicate that the upstream class III phosphatidylinositol 3-kinase (PI3K) complex, but not LC3 conjugation machinery, is utilized in DMV formation. Both chemical and genetic inhibition of the PI3K complex lead to significant reduction in DMVs, as well as viral replication. Elucidating the role of autophagy machinery in DMV formation during astrovirus infection reveals a potential target for therapeutic intervention for immunocompromised patients.

IMPORTANCE These studies provide critical new evidence that astrovirus replication requires formation of double-membrane vesicles, which utilize class III phosphatidylinositol 3-kinase (PI3K), but not LC3 conjugation autophagy machinery, for biogenesis. These results are consistent with replication mechanisms for other positive-sense RNA viruses suggesting that targeting PI3K could be a promising therapeutic option for not only astrovirus, but other positive-sense RNA virus infections.

KEYWORDS astrovirus, autophagy, class III PI3K, double-membrane vesicle, replication organelle

Astroviruses are positive-sense, single-stranded, non-enveloped RNA viruses that cause disease in a variety of mammals and birds (1–4). In humans, infection is often associated with gastrointestinal symptoms such as nausea, vomiting, loss of appetite, stomachaches, and diarrhea (4–7). However, astrovirus infections can also result in fatal encephalitis, particularly in immunocompromised individuals (2, 7–12). Astrovirus infections are typically under-reported despite high prevalence (13, 14), and there are significant gaps in knowledge about astrovirus pathogenesis including the mechanisms behind viral replication.

Many positive-sense, single-stranded RNA viruses including hepatitis C virus (HCV), coronaviruses, picornaviruses, and noroviruses utilize double-membrane vesicles (DMVs) as replication chambers during infection. These replication organelles shield viral RNA from recognition by intracellular pattern recognition receptors that could alert the immune system (15–22). It has been suggested that DMVs form with the aid of autophagy machinery. Generally, autophagy serves as the recycling system of the cell. During

Editor Felicia Goodrum, The University of Arizona, Tucson, Arizona, USA

Address correspondence to Stacey Schultz-Cherry, Stacey.Schultz-Cherry@StJude.org.

The authors declare no conflict of interest.

See the funding table on p. 16.

Received 10 July 2023
Accepted 11 July 2023
Published 5 September 2023

autophagy, double-membrane vesicles called autophagosomes deliver cytoplasmic material to the lysosome for degradation. Autophagy can also be selective, targeting specific cargo such as depolarized mitochondria, damaged endoplasmic reticulum (ER) fragments, and others. The lysosome then fuses with the autophagosome, and cargo is degraded due to lysosomal enzymatic activity and acidic pH, recycling it for further use by the cell (23–26). The formation of the autophagosome can vary depending on whether the pathway is canonical or non-canonical. The canonical autophagy pathway involves machinery first characterized in starvation-induced autophagy, including the ULK1 pre-initiation complex, the class III phosphatidylinositol 3-kinase (PI3K) complex required for production of phosphatidylinositol 3-phosphate (PI3P), and the LC3 conjugation system required for autophagosome maturation. Non-canonical pathways may utilize only some parts of the originally characterized autophagy machinery (27). Regardless of the pathway, these cellular components are often manipulated by viruses during infection to enhance viral replication.

Positive-strand RNA viruses can hijack components of the autophagy machinery to form DMVs, which share characteristics with autophagosomes. However, viral-induced DMVs can be distinct from autophagosomes. They are not always delivered to lysosomes for degradation, tend to be smaller in size compared to autophagosomes, and importantly, canonical autophagy machinery is not necessarily involved in the formation of these vesicles (15, 17–20, 22). Notably, viruses can induce the formation of DMVs from the ER, Golgi apparatus, mitochondria, and other sites in the cell, which may have virus-specific implications for antiviral therapies (19, 22, 28). Recent evidence has shown that DMV formation is independent of LC3 lipidation machinery in both severe acute respiratory syndrome coronavirus 2 (SARS-CoV-2) and HCV infection; instead, both viruses appear to rely on the PI3K complex for formation of PI3P in DMV membranes (21, 29). Coxsackievirus B3, on the other hand, induces DMV formation that is independent of PI3K and ULK1 machinery, relying instead upon PI4KIIIβ for formation of these vesicles (30–32). Although electron microscopy images have shown association of lamb astrovirus with DMVs in lamb intestines (33), the role of autophagy in astrovirus infection has remained uncharacterized in both humans and animal models.

In the present study, we find that DMVs formed during astrovirus infection rely on a PI3K-dependent, LC3-independent autophagy pathway and may originate from the ER. This machinery is targetable, and using an autophagy-specific PI3K inhibitor and specific small interfering RNA (siRNA) knockdown significantly reduces DMV formation and astrovirus replication. Targeting DMV formation through inhibition of the PI3K complex during astrovirus infection offers a potential therapy for astrovirus infection, and this therapy may further be applicable to other positive-sense RNA viruses.

RESULTS

Astrovirus induces DMV formation during replication

A previous study showed that astrovirus infection in lambs resulted in the formation of DMVs (33). To determine if this was also true with human astroviruses, we performed transmission electron microscopy (TEM) on mock-inoculated and human astrovirus-1 (HAstV-1)-infected Caco-2 cells at 8, 12, 24, and 36 h post-infection (hpi). Beginning at 24 hpi, HAstV-1-infected cells had widespread formation of DMVs of approximately 200–500 nm in size compared to mock-inoculated Caco-2 cells (Fig. 1A). The DMVs were associated with HAstV-1 virions. Induction of DMV formation was dependent on productive viral replication, as UV-inactivated virus failed to induce DMVs (Fig. 1B).

Inhibition of the PI3K complex significantly reduces astrovirus replication

Like autophagosomes, DMVs have a double membrane and can utilize components of the autophagy machinery during formation. A recent study of SARS-CoV-2 and HCV replication demonstrated that the PI3K complex involved in the formation of PI3P during autophagy is necessary to the formation of DMVs during viral replication (21). One study

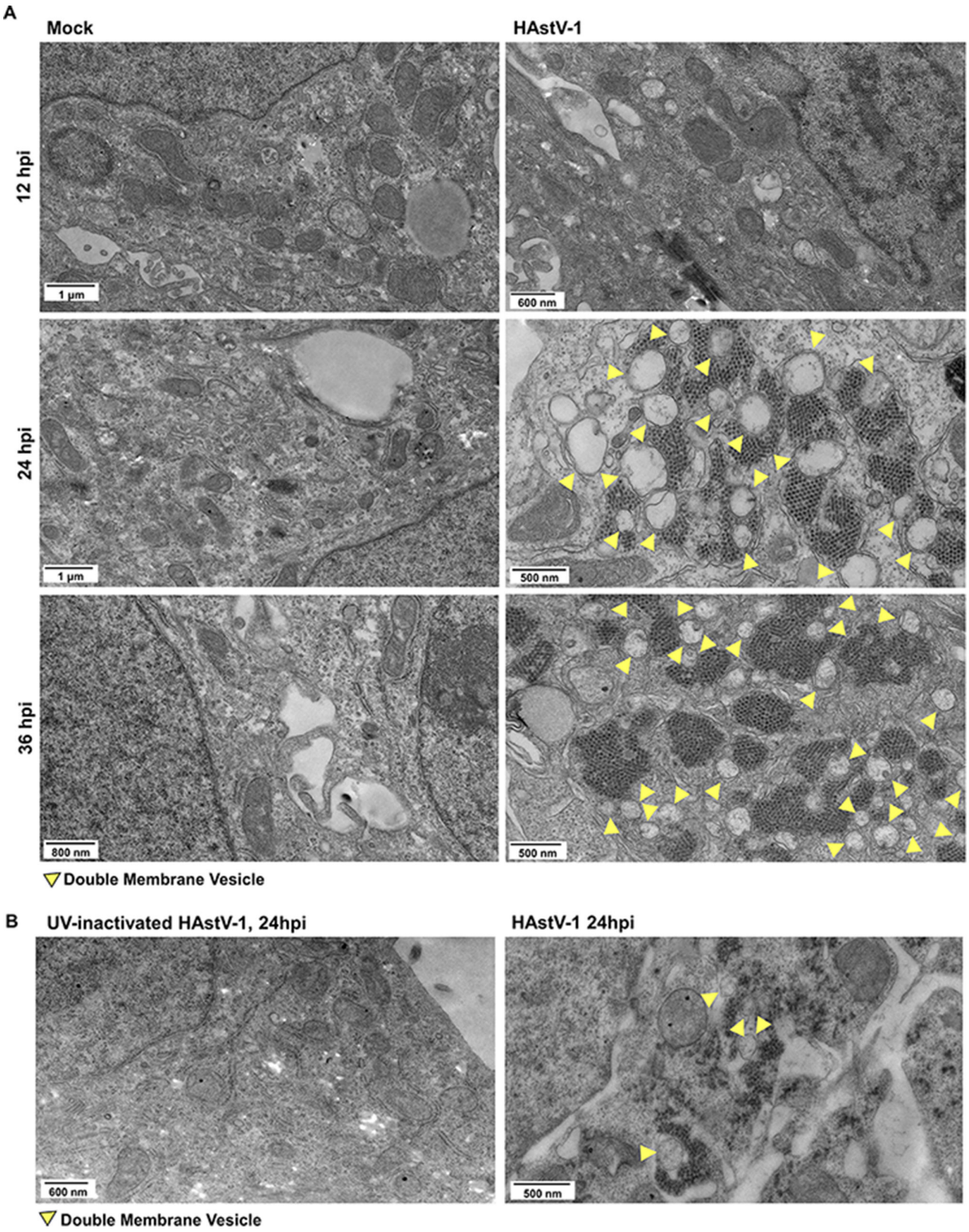

FIG 1 Astrovirus associates with DMVs during infection. (A) TEM images of mock-inoculated or HAstV-1-infected Caco-2 cells at 12, 24, and 36 hpi. (B) TEM images of UV-inactive HAstV-1-inoculated Caco-2 cells and HAstV-1-infected Caco-2 cells at 24 hpi. (A and B) Yellow arrows indicate DMVs.

showed that pan-PI3K inhibitors wortmannin and LY294002 were effective in reducing HAstV-1 infection (34, 35). However, this study did not address which PI3K complex is necessary for astrovirus infection or which part of the replication pathway is affected by

inhibition. To test whether the autophagy-specific class III PI3K complex is required for astrovirus replication, we infected Caco-2 cells with HAstV-1 and treated Caco-2 cells with PIK-III, a specific class III phosphatidylinositol 3-kinase (PI3KC3) complex inhibitor, or DMSO (dimethyl sulfoxide) at 1 hpi. At 24 hpi, the cells were fixed for TEM. PIK-III treatment significantly reduced the presence of DMVs and viral particles at 24 hpi, suggesting that the PI3K complex may support viral replication via formation of DMVs (Fig. 2A).

To determine whether inhibition of the PI3K complex affects astrovirus replication, we infected Caco-2 cells with HAstV-1 and treated cells with varying concentrations of PIK-III or DMSO at 2 h pre-infection or 1 hpi. At 24 hpi, we fixed and stained the cells for HAstV-1 capsid or dsRNA. We observed significantly less capsid and dsRNA staining in the PIK-III-treated Caco-2 cells compared to the DMSO control at 24 hpi, and this difference was dose-dependent. Pre-infection treatment with PIK-III was not significantly different from post-infection treatment (Fig. 2B; Fig. S1a). We then repeated the experiment, collecting cells and supernatants at 24 hpi, and extracted RNA to quantify HAstV-1 genome copies. Similarly, we found that PIK-III decreased HAstV-1 genome copies in both cell lysates and supernatant significantly in a dose-dependent manner (Fig. 2C). Then, using supernatants from these cells, we found that cells that had been treated with PIK-III after HAstV-1 infection produced significantly less infectious virus than cells treated with DMSO (Fig. 2D). Finally, to determine whether this PI3K-dependent replication mechanism expands to other human astrovirus genotypes, we infected Caco-2 cells with the human astrovirus VA-1 strain and treated them with varying concentrations of PIK-III or DMSO at 1 hpi. At 48 hpi, we fixed and stained the cells for VA-1 capsid and observed significantly less VA-1 infection in Caco-2 cells treated with PIK-III compared to DMSO controls in a dose-dependent manner (Fig. S1b). These experiments suggest that the PI3K complex aids in viral replication through formation of DMVs.

To confirm these results, we knocked down a key component of PI3KC3, Beclin. Caco-2 cells were transfected with siRNA for Beclin or a control siRNA at about 70% confluence. After 2 days, cells were infected with HAstV-1. At 24 hpi, cells were collected, and genome copies were measured. Caco-2 cells transfected with siBeclin had at least 50% less Beclin expression and had significantly reduced genome copies of astrovirus compared to siControl (Fig. 3A and B). The experiment was repeated, and cells were fixed at 24 hpi for imaging. Cells treated with siBeclin had significantly less astrovirus capsid and double-stranded RNA at 24 hpi compared to siControl, further supporting a role for the PI3KC3 complex in astrovirus replication (Fig. 3C and D).

LC3 conjugation machinery is not required for astrovirus replication

To determine whether astrovirus-induced DMV formation was accompanied by an upregulation in other autophagy machinery, we utilized a real-time polymerase chain reaction (RT-PCR) array (custom Qiagen RT^2 Profiler) of canonical and alternative autophagy-related genes, as well as cell death-related genes, vesicular trafficking genes, and exosome-related genes. At 24 hpi, there was a significant upregulation in autophagy-related genes in HAstV-1 infected cells compared to the 2 hpi time point including *ULK1, AMBRA1, UVRAG*, *SQSTM1*, and *GABARAPL1,* in addition to *IDO1*. However, *MAP1LC3A, ATG5,* and *ATG7* genes associated with LC3 conjugation machinery were unchanged (Fig. 4A).

Immunoblots of lysates from mock-inoculated and HAstV-1-infected Caco-2 cells confirmed that ATG5 and ATG7 were not upregulated (Fig. 4B). Given that we did not observe an upregulation of ATG5 and ATG7, we hypothesized that astrovirus-induced DMVs form independently of LC3 conjugation machinery. To test this, we repeated the siRNA experiment, knocking down Atg5 to disrupt LC3 conjugation machinery. Atg5 was significantly reduced translationally in siATG5 cells compared to siControl, and there was no difference in astrovirus genome copies in siATG5 cells compared to siControl (Fig. 4C; Fig. S2a). In addition, in siATG5-treated Caco-2 cells, there was no difference in capsid or double-stranded RNA at 24 hpi compared to siControl (Fig. 4D; Fig. S2c and d). To

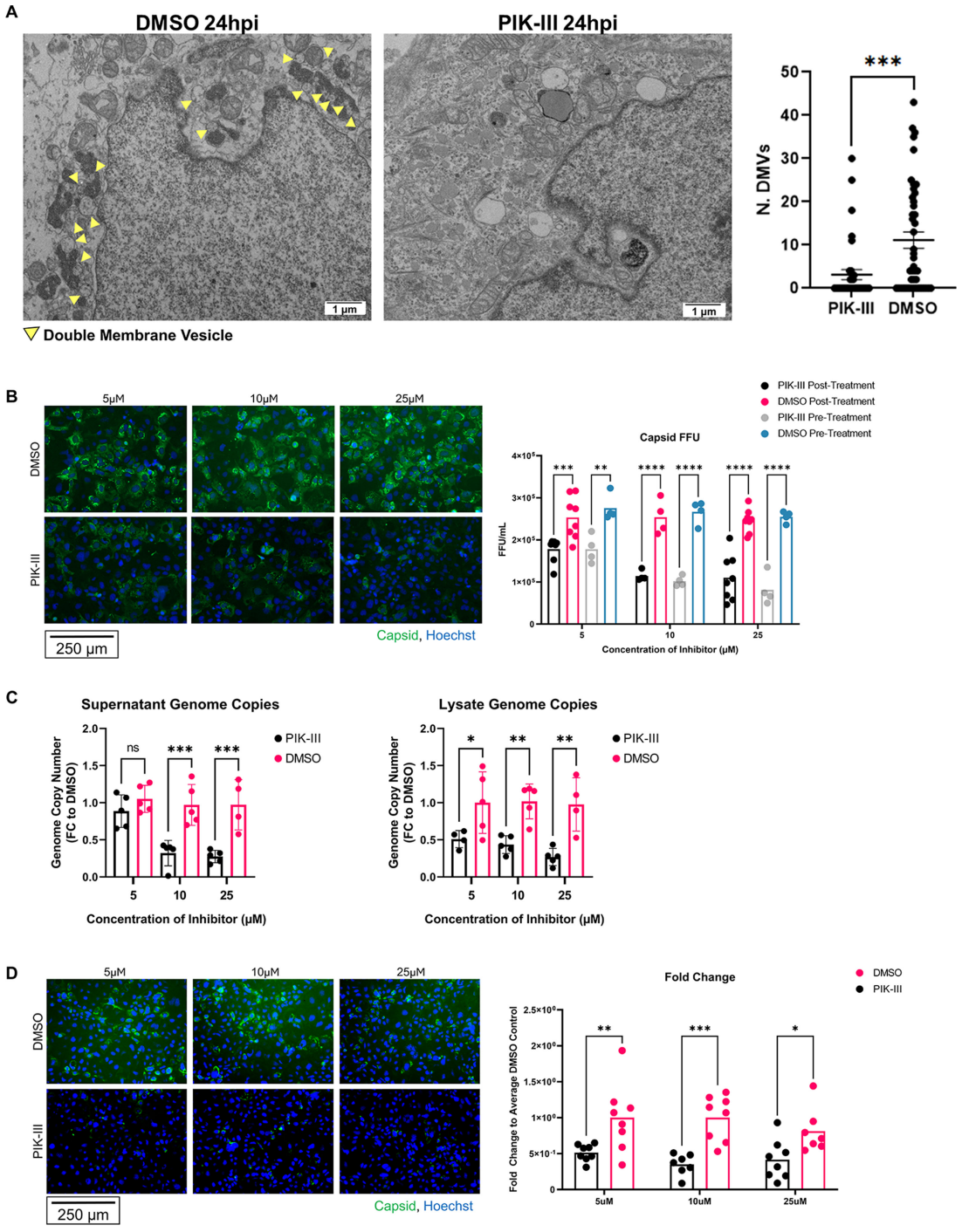

FIG 2 Inhibition of the PI3K complex reduces astrovirus replication. (A) TEM of PIK-III-treated and DMSO control HAstV-1-infected Caco-2 cells at 24 hpi and quantification of number of DMVs. Arrows indicate DMVs. Statistical analysis was by unpaired two-tailed *t*-test. ***, $P \leq 0.001$. (B) HAstV-1-infected Caco-2 cells were either pre-treated for 2 h prior to infection or treated 1 hpi with 5, 10, or 25 µM PIK-III or DMSO control. EVOS microscope images represent Caco-2 cells treated at 1 hpi, with astrovirus capsid in green and nucleus (Hoechst) in blue. Quantification shows focus-forming unit (FFU) of samples treated 2 h before infection and 1 hpi with statistical analysis by two-way analysis of variance (ANOVA) followed by Tukey's multiple comparison test. (C) Genome copy number of human astrovirus in cell lysate and supernatant at 24 hpi from HAstV-1-infected Caco-2 cells treated with 5, 10, or 25 µM PIK-III or DMSO control at 1 hpi with statistical analysis by two-way ANOVA followed by Tukey's multiple comparison test. (D) Supernatants from HAstV-1-infected Caco-2 cells treated with 5, 10, or 25 µM PIK-III or DMSO control were collected and trypsin-treated at 24 hpi. Supernatants were used to infect Caco-2 cells. EVOS images show astrovirus capsid (green) and nucleus (Hoechst, blue). Quantification of FFU fold change to average DMSO control is shown. *, $P \leq 0.05$; **, $P \leq 0.01$; ***, $P \leq 0.001$.

validate these results, we utilized Huh-7.5 cells expressing doxycycline-inducible RavZ cysteine protease. RavZ has been shown to cleave LC3, impairing its ability to become conjugated to phosphatidylethanolamine (PE), leading to a reduction in autophagosome formation (36, 37). After validating that induction of RavZ expression decreases LC3 levels, as shown by immunoblot (Fig. S2b), we induced RavZ activity and infected the cells with HAstV-1. After infection with HAstV-1, we collected RNA from cells and supernatants for quantification of HAstV-1 genome copies at 24 hpi. There was no change in genome copies in the absence of LC3 lipidation activity, suggesting that LC3

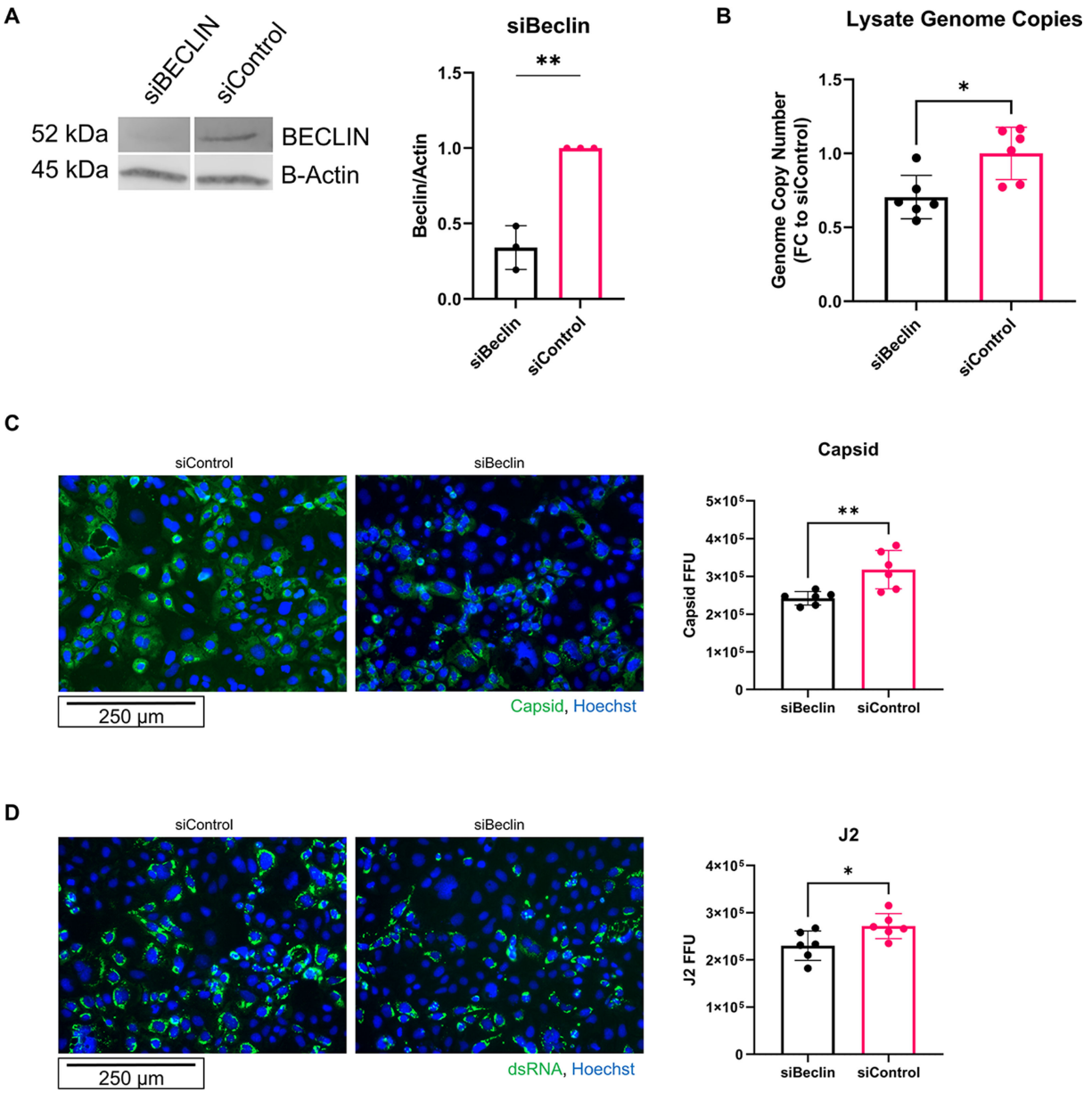

FIG 3 Knockdown of Beclin1 reduces astrovirus replication. (A) Representative immunoblot and quantification of immunoblots for Beclin expression after siBeclin knockdown compared to siControl with statistical analysis by unpaired two-tailed *t*-test. (B) Genome copy number of human astrovirus in cell lysate at 24 hpi from HAstV-1-infected Caco-2 cells treated with either siBeclin or siControl with statistical analysis by unpaired two-tailed *t*-test. (C and D) Caco-2 cells were treated with siBeclin or siControl 24 h after plating, once cells had reached 70% confluency. At 48 h post-treatment with siRNAs, Caco-2 cells were infected with HAstV-1. At 24 hpi, Caco-2 cells were fixed. (C) EVOS microscope images show astrovirus capsid in green and nucleus (Hoechst) in blue. Quantification shows FFU with statistical analysis by unpaired two-tailed *t*-test. (D) EVOS microscope images show astrovirus double-stranded RNA (J2) in green and nucleus (Hoechst) in blue. Quantification shows FFU with statistical analysis by unpaired two-tailed *t*-test.

lipidation machinery and production of LC3-II are not required for astrovirus replication (Fig. 4E)

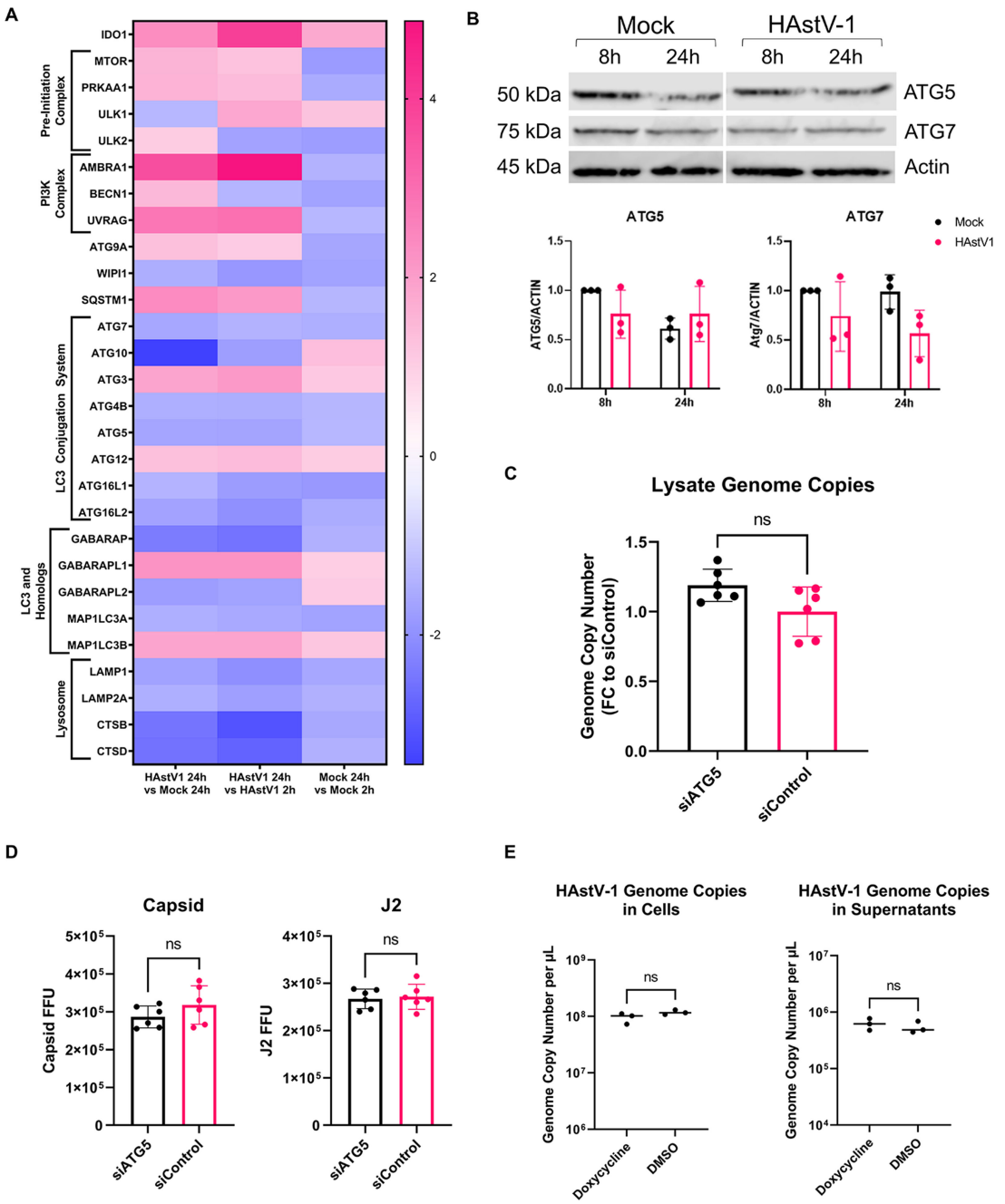

FIG 4 LC3 conjugation machinery is not required for astrovirus replication. (A) Heat map of gene fold regulation from RT^2 profiler data set. (B) Immunoblot showing expression of ATG5 and ATG7 at 8 and 24 hpi in mock-inoculated and HAstV-1-infected Caco-2 cell lysates. Quantification of 8-h and 24-h time points was performed with statistical analysis by two-way ANOVA followed by Tukey's multiple comparison test. (C) Genome copy number of human astrovirus in cell lysate at 24 hpi from HAstV-1-infected Caco-2 cells treated with either siATG5 or siControl with statistical analysis by unpaired two-tailed *t*-test. (D) Caco-2 cells were treated with siATG5 or siControl 24 h after plating, once cells had reached 70% confluency. At 48 h post-treatment with siRNAs, Caco-2 cells were infected with HAstV-1. At 24 hpi, Caco-2 cells were fixed. Quantification shows FFU for astrovirus capsid and double-stranded RNA (J2) with statistical analysis by unpaired two-tailed *t*-test. (E) Genome copies per microliter of astrovirus in cell lysate and supernatant RNA collected from HAstV-1-infected Huh-7.5 cells, where cells treated with doxycycline had induced RavZ protease activity. Statistical analysis was by unpaired two-tailed *t*-test.

Transcriptional changes in autophagy machinery occur in astrovirus-infected cells *in vitro* and *in vivo*

Finally, to determine if there were changes in autophagy gene expression specifically in astrovirus-infected cells, we performed single-cell RNA sequencing on astrovirus-infected Caco-2 cells at 4, 8, and 24 hpi (Table 1). At 24 hpi, most cells in the HAstV-1-infected Caco-2 sample were infected and clustered together (Fig. 5A). To characterize differences

TABLE 1 Top 15 upregulated genes in mock, infected, and bystander clusters for the HAstV-1 Caco-2 single-cell RNA sequencing data set at 24 hpi

Gene	Cluster	avg_log2FC	pct.1	pct.2	p_val_adj
ITM2B	Mock	0.656933	0.785	0.428	0
RPL17	Mock	0.529021	0.943	0.716	0
S100A10	Mock	0.52348	0.916	0.681	0
CD99	Mock	0.5072	0.972	0.786	0
H2AFZ	Mock	0.701308	0.649	0.268	8.89E−265
EPCAM	Mock	0.635118	0.698	0.345	1.78E−252
MIF	Mock	0.636467	0.625	0.27	2.30E – 220
SCD	Mock	0.563748	0.689	0.377	8.00E−201
PTMA	Mock	0.548704	0.725	0.397	1.02E−186
NME2	Mock	0.536384	0.663	0.357	1.60E−171
CST3	Mock	0.544066	0.678	0.387	3.19E−171
TUBA1B	Mock	0.565624	0.604	0.28	6.11E−167
PDIA6	Mock	0.534388	0.433	0.15	8.62E−149
PFN1	Mock	0.526555	0.53	0.247	9.26E−148
TPI1	Mock	0.510377	0.522	0.244	1.72E−138
HAstV1	Infected	2.749525	1	0	0
ZC3HAV1	Infected	1.110522	0.792	0.255	0
IFIT3	Infected	1.061962	0.517	0.039	0
IRF1	Infected	0.981695	0.523	0.041	0
IFI6	Infected	0.981588	0.784	0.3	0
DTX3L	Infected	0.967167	0.776	0.276	0
KLF6	Infected	0.93654	0.687	0.229	0
APOL2	Infected	0.933543	0.558	0.129	0
HELZ2	Infected	0.92706	0.509	0.04	0
DDX58	Infected	0.89635	0.464	0.041	0
PARP14	Infected	0.877263	0.722	0.276	0
ISG15	Infected	0.87406	0.495	0.058	0
TFAP2C	Infected	0.859227	0.731	0.335	0
IFIT2	Infected	0.856451	0.342	0.012	0
STAT2	Infected	0.849258	0.8	0.407	0
HMGB1	Bystander	0.315939	0.894	0.735	4.06E−19
HMGN2	Bystander	0.336253	0.82	0.657	3.40E−18
TUBA1B	Bystander	0.427122	0.707	0.439	6.20E−18
SSR3	Bystander	0.329197	0.749	0.6	9.21E−17
EBP	Bystander	0.31393	0.848	0.688	1.71E−15
PARP14	Bystander	0.405334	0.71	0.46	5.39E−15
SYNC	Bystander	0.401247	0.587	0.372	3.74E−14
AC091607.2	Bystander	0.349163	0.668	0.496	2.80E−12
TUBB	Bystander	0.381438	0.541	0.337	4.94E−12
PTMA	Bystander	0.315548	0.731	0.562	2.88E−11
RRM2	Bystander	0.407369	0.516	0.304	2.98E−11
PA2G4	Bystander	0.339074	0.65	0.439	5.45E−11
IFI6	Bystander	0.367067	0.746	0.501	1.96E−10
IFIT1	Bystander	0.327753	0.325	0.154	2.79E−10
MYADM	Bystander	0.347887	0.583	0.412	4.98E−09

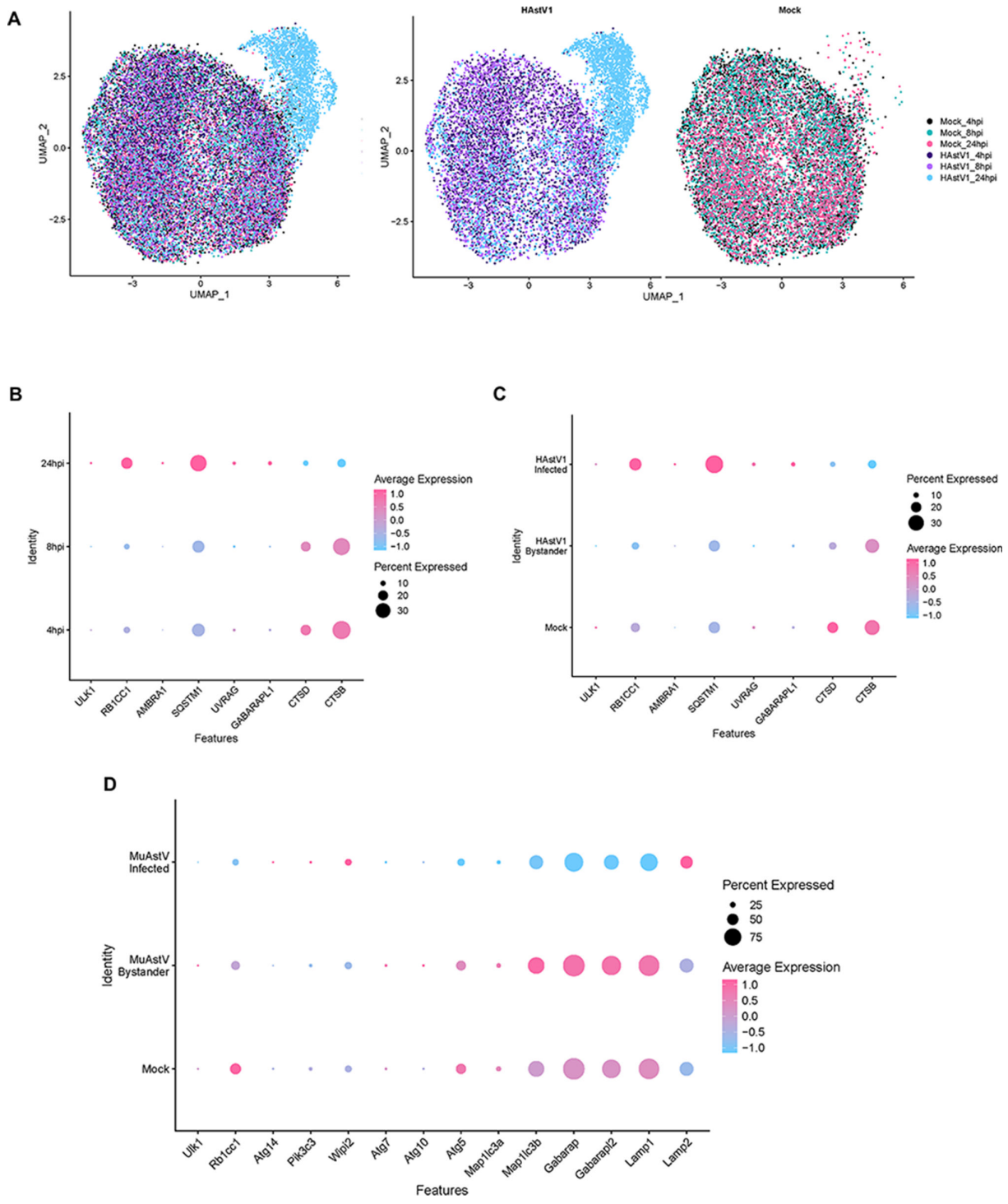

FIG 5 Changes in autophagy-related genes in astrovirus-infected cells in human and murine single-cell RNA sequencing data sets. (A) Uniform Manifold Approximation and Projection (UMAP) showing clustering of HAstV-1 and mock 4, 8, and 24 hpi samples. (B) Dot plot showing percent expression and average expression of autophagy-related genes in HAstV-1-infected Caco-2 cell samples at 4, 8, and 24 hpi from 10× single-cell RNA sequencing data set. (C) Dot plot showing percent expression and average expression of autophagy-related genes in HAstV-1-infected Caco-2 cells, HAstV-1-uninfected (bystander) Caco-2 cells, and mock-inoculated Caco-2 cells at 24 hpi from 10× single-cell RNA sequencing data set. (D) Dot plot showing percent expression and average expression of autophagy-related genes in murine astrovirus (MuAstV)-infected, MuAstV-uninfected (bystander), and mock-inoculated cells at 24 hpi from 10× single-cell RNA sequencing murine astrovirus data set (13).

between samples at 24 hpi, we utilized Gene Ontology (GO), Kyoto Encyclopedia of Genes and Genomes (KEGG), and Hallmark pathway analyses to determine differences between gene expression pathways in mock, astrovirus-infected, and bystander cell types (Fig. S3). Next, we explored whether autophagy-related genes were dysregulated in the data set across time points and between infected, bystander, and mock groups. The single cell RNA sequencing (scRNA-seq) data set confirmed that the regulation of PI3KC3-associated genes in HAstV-1-infected samples followed the same pattern as the RT-PCR array, increasing over time (Fig. 5B). In addition, upregulation in upstream autophagy pathway genes occurred only in astrovirus-infected but not bystander cells (Fig. 5C).

Using a single-cell RNA sequencing data set previously collected by our laboratory (13), we found that intestines from murine astrovirus-infected mice had an upregulation in *Pik3c3* in Murine Astrovirus (MuAstV)-infected but not bystander cells. This data set showed a downregulation in *Map1lc3a* and its homologs *Gabarap* and *Gabarapl2*, as well as *Ulk1, Rb1cc1, Atg7, Atg10, Atg5,* and *Lamp1* in infected but not bystander cells (Fig. 5D). This suggests that murine astrovirus replication could also utilize the PI3K complex but not the LC3 conjugation machinery, for replication *in vivo*. Future work will address the involvement of the PI3K complex in murine astrovirus replication and whether PI3K could be a therapeutic target for astrovirus infection spanning different species. These experiments provide evidence that astrovirus infection upregulates certain, but not all, components of autophagy machinery *in vitro* and *in vivo* to facilitate viral replication.

DISCUSSION

Here, we show that astrovirus infection induces formation of DMVs, and this process is replication-dependent. Formation of these DMVs also requires some, but not all, canonical autophagy machinery. We demonstrate that astrovirus uses the autophagy-specific PI3KC3 complex for formation of DMVs. The PI3K complex initiates phagophore formation and production of PI3P during canonical autophagy (27, 38, 39). Inhibiting this complex either chemically or through siRNA knockdown of complex component Beclin1 greatly reduces astrovirus replication and infectious virus production, as well as formation of DMVs as seen by electron microscopy. VA1 infection is also significantly reduced upon chemical inhibition of PI3KC3, suggesting a strain-spanning mechanism for astrovirus replication.

Previous studies of positive-sense RNA virus replication have shown that canonical LC3 machinery may not be necessary for RNA virus replication using DMVs (21, 29). The LC3 conjugation system is indispensable for canonical, starvation-induced autophagy. It consists of *E1*- and *E3*-like proteins ATG5 and ATG7, which work together to conjugate LC3-I to PE to form LC3-II. This crucial step leads to autophagosome maturation (27, 38). Our work is consistent with previous literature, as we also observed that inhibition of LC3 machinery in multiple cell types does not affect astrovirus replication. These data are consistent with recent studies showing that SARS-CoV-2 and HCV utilize the PI3K complex, but not LC3 conjugation machinery for DMV formation and replication (21, 29). Our work suggests that early parts of autophagy machinery are essential for DMV formation, while LC3 conjugation is not required. This is supported by transcriptional data from single-cell RNA sequencing data sets, showing that astrovirus-infected cells upregulate PI3K-associated genes, while bystander and mock-inoculated cells do not in both human and murine data sets. This suggests a species-spanning mechanism.

Without LC3 involvement in the formation of DMVs, it is possible that an LC3 homolog, such as the significantly upregulated GABARAPL1, could be active in the formation of DMVs during astrovirus replication. Notably, while inhibition of PI3K significantly reduces astrovirus replication, it does not ablate replication entirely. One possible explanation for this is that other phosphatidylinositol kinases are also involved in the formation of these DMV replication organelles, such as PI4K (19, 21, 22, 24). Use of a PI4K inhibitor during astrovirus infection could determine whether this is the case.

While it is clear that formation of DMVs during astrovirus infection is replication-dependent, it is not yet determined which parts of the astrovirus genome are necessary for inducing formation of DMVs. Nonstructural proteins alone from other viruses such as HCV and SARS-CoV-2 are sufficient for induction of DMV formation (40–42). Little is known about the function of astrovirus nonstructural proteins, and it is likely that they play a role in DMV formation (43, 44).

Altogether, our results indicate that astrovirus replication relies upon the formation of DMVs using early autophagy machinery, including the PI3K complex, but not LC3 conjugation machinery. Future studies will address whether the PI3K complex is necessary for astrovirus infection in brain cells, leading to encephalitis in immunocompromised populations. These results emphasize how distinct positive-strand RNA viruses utilize similar mechanisms of replication. Although SARS-CoV-2, HCV, and HAstV-1 are different, their common use of the PI3K machinery implies the possibility of a conserved therapeutic target for many positive-sense RNA viruses. Understanding these replication mechanisms will help to determine future antiviral therapies.

MATERIALS AND METHODS

Cells and virus propagation

Caco-2 human intestinal adenocarcinoma cell line was obtained from ATCC (HTB-37). Cells were grown in Corning minimum essential medium containing 20% fetal bovine serum (FBS; HyClone), GlutaMax (Gibco), 1 mM sodium pyruvate (Gibco), and penicillin-streptomycin (Fisher).

The Huh-7.5 RavZ inducible cell line was a generous gift from Brett Lindenbach's lab at the Yale School of Medicine. These cells were grown in Dulbecco's modified Eagle medium (DMEM) (ThermoFisher) containing 10% FBS (HyClone) and 3 µg/mL puromycin (Invitrogen).

HAstV-1 and VA1 lab-adapted viral stocks were propagated in Caco-2 cells. Viral titer was quantified using focus-forming unit assay (FFU) as previously described (45). For UV inactivation experiments, a UV cross-linker was utilized to subject HAstV-1 to 100 mJ/cm^2, and inactivation was confirmed using FFU assay.

Transmission electron microscopy

Caco-2 cells were plated in a six-well plate (3.5×10^5). After 46 h, appropriate samples were treated with 10 µM PIK-III or DMSO. Two hours later, cells were inoculated with supernatants taken from HAstV-1 (multiplicity of infection (MOI) 10) or mock-inoculated Caco-2 cells in serum-free media for 1 h. Following virus adsorption, inoculum was replaced with either fresh media, media containing 10 µM PIK-III, or media containing DMSO. At 8, 12, 24, or 36 hpi, cells were fixed in 2.5% glutaraldehyde/2% paraformaldehyde (PFA) in 0.1 M Cacodylate Buffer. Following fixation, samples were post fixed in osmium tetroxide and contrasted with aqueous uranyl acetate. Samples were dehydrated by an ascending series of ethanol to 100% followed by 100% propylene oxide. Samples were infiltrated with EmBed-812 and polymerized at 60°C. Embedded samples were sectioned at ~70 nm on a Leica (Wetzlar, Germany) ultramicrotome and examined in a ThermoFisher Scientific (Hillsboro, OR) TF20 transmission electron microscope at 80 kV. Digital micrographs were captured with an Advanced Microscopy Techniques (Woburn, MA, USA) imaging system. Unless otherwise indicated, all reagents are from Electron Microscopy Sciences (Hatfield, PA, USA).

RT^2 profiler

Caco-2 cells were plated in a six-well plate (3.5×10^5). After 48 h, cells were inoculated with supernatants taken from HAstV-1 (MOI 10) or mock-inoculated Caco-2 cells in serum-free media for 1 h. Following virus adsorption, the inoculum was replaced with fresh media. At 2, 8, and 24 hpi, cell supernatants were collected in TRIzol for liquid

samples (LS). Cells were collected in TRIzol, and RNA was extracted from all samples per manufacturer's instructions. RNA quality was checked using Thermo Scientific NanoDrop 2000 per manufacturer's instructions. Then, qRT-PCR was performed on supernatant RNA to determine genome copies of HAstV-1 in supernatants, as previously described (46). We confirmed that genome copies of astrovirus increased in HAstV-1-infected cell supernatants over time, and no genome copies were detected in mock-inoculated cell supernatants. Then, RNA from cells was reverse transcribed using the RT^2 First Strand Kit from Qiagen (Qiagen 330401). After cDNA was collected, it was utilized with SYBR Green qPCR Mastermix (Qiagen 330500) in a custom-designed real-time RT^2 Profiler PCR Array (Qiagen 330171). Cycle threshold (CT) values were collected, and data analysis was performed using Qiagen's data analysis web portal (http://www.qiagen.com/geneglobe). In addition, we have found that astrovirus induces epithelial to mesenchymal transition, reducing epithelial markers on Caco-2 cells later in infection (47). It has also been shown that IDO1 is upregulated during astrovirus infection (48). Thus, *IDO1* and *EpCAM* were included in the panel to verify normal cellular response to astrovirus infection.

Mock and HAstV-1-treated samples were designated as control and test groups, respectively. All samples passed quality checks. Reference genes were included in the RT^2 panel, and data were normalized to these genes. The Qiagen data analysis protocol included fold change/regulation calculations based on ΔΔCT calculations. Statistical analysis on the Qiagen web portal utilized a Student's *t*-test to calculate *P*-values, where parametric, unpaired, two-sample equal variance, two-tailed distribution was utilized.

10× single-cell RNA sequencing sample preparation

Caco-2 cells were plated in a six-well plate (3.5×10^5). Samples were assigned to wells corresponding to 4, 8, or 24 h post-infection. At 48 h post-plating, 24 hpi cell wells were inoculated with supernatants taken from HAstV-1 (MOI 10) or mock-inoculated Caco-2 cells in serum-free media for 1 h. After virus adsorption, the inoculum was replaced with fresh media. At 64 h post-plating, 8 hpi cell wells were inoculated with supernatants taken from HAstV-1 (MOI 10) or mock-inoculated Caco-2 cells in serum-free media for 1 h. After virus adsorption, the inoculum was replaced with fresh media. At 68 h post-plating, 4 hpi cell wells were inoculated with supernatants taken from HAstV-1 (MOI 10) or mock-inoculated Caco-2 cells in serum-free media for 1 h. After virus adsorption, the inoculum was replaced with fresh media. At 72 h post-plating, all cells were washed with phosphate buffered saline (PBS) and harvested using trypsin. Cells were filtered through at 70 µm cell strainer. Cells were spun down at 1,200 rpm for 10 min at 4°C. Cells were washed in cell wash buffer (1% bovine serum albumin (BSA) in PBS) and spun down again at 1,200 rpm for 10 min at 4°C. Finally, cells were resuspended in 50 µL of cell wash buffer and counted using a hemocytometer. Cells were resuspended in appropriate volume to reach 1,000 cells/µL. Next, 9,000 cells were loaded onto the 10× Genomics Chromium controller for partitioning of single cells into gel beads with a goal of recovering 6,000 cells. Next, using a 10× Genomics 3′ Gene Expression Kit (version 3.1) according to manufacturer's instructions, single-cell transcriptomics libraries were produced. Libraries were sequenced using Illumina NovaSeq 2000 at suggested sequencing lengths and depths.

10× single-cell RNA sequencing analysis

The 10× transcriptomics data were first processed using CellRanger count (version 6.1.1, 10× Genomics). GRCh38 was used as our reference, which was altered to include the human astrovirus 1 genome (accession ID MK059949.1). Samples were aggregated and normalized by the median number of mapped reads per identified cell using CellRanger aggr. Normalized gene expression matrices were then imported into Seurat (version 4.1.1) for downstream analysis and data visualization.

Data were first filtered by excluding any gene that was not present in at least 0.1% of total called cells (23 cells). Cells that exhibited extremes in the total number of transcripts expressed (>6,000), the total number of genes expressed (<400 or >3,000),

or mitochondrial gene expression (>8%) were then excluded from downstream analyses. Data were log-normalized using default parameters. We identified the top 2,000 variable features using the variance-stabilizing transformation (VST) method.

The fastMNN algorithm was then utilized to integrate data sets from distinct libraries, effectively minimizing subject- and sample-specific differences in order to identify similar transcriptional subsets. The first 25 fastMNN dimensions were used for Uniform Manifold Approximation and Projection (UMAP) dimensionality reduction and for nearest-neighbor graph construction for identifying transcriptional clusters in Seurat. Markers for each cluster were identified using FindAllMarkers function (min.pct = 0.25, logfc.threshold = 0.25).

We also generated a subset for 24 hpi samples alone. This subset was processed as described above. We split cells in the 24 hpi infected group to two sub-groups: "HAstV1-Infected" included cells that detected at least one astrovirus gene, "HAstV1-Bystander" included cells that did not detect astrovirus gene. Over-representation analysis was performed using clusterProfiler (function: Function enrichGO, enrichKEGG, and enricher) to explore the biological and molecular functions of each group (49).

Immunofluorescent staining

For PIK-III experiments, Caco-2 cells were plated in a 96-well plate (2.5×10^4). At 46 h post-plating, appropriate wells were treated with 5, 10, or 25 µM PIK-III or DMSO control. At 48 h post-plating, cells were inoculated with supernatants taken from HAstV-1 (MOI 10) or mock-inoculated Caco-2 cells in serum-free media for 1 h. Following virus adsorption, the inoculum was replaced with fresh media or media containing 5, 10, or 25 µM PIK-III or DMSO control. At 24 hpi, cells were fixed in 100% methanol. Cells were washed in PBS and incubated in primary antibody solution containing astrovirus capsid monoclonal antibody 8e7 (Invitrogen MA5-16293) at 1:100 in 1% normal goat serum (NGS)/PBS for 1 h at room temperature. Cells were washed in PBS. Cells were incubated in secondary antibody solution containing Alexa Fluor 488 goat anti-Mouse (Invitrogen A10680) at 1:1,000 and and Hoechst (ThermoFisher H3569) at 1:2,000 in 1% NGS/PBS for 45 min in the dark. Cells were again washed in PBS. Samples were imaged using the EVOS FL cell imaging system and analyzed using ImageJ 2.9.0/1.53t software. FFU was calculated as previously described (45). The same method was used for supernatants from PIK-III- and DMSO-treated cell supernatants used to infect fresh Caco-2 cells in a 96-well plate.

For siRNA experiments, Caco-2 cells were plated in a 96-well plate (1.5×10^4). At 24 h post-plating, appropriate wells were treated with 15 µM siRNA (Atg5, Beclin, or Control siRNA). Cells were allowed to incubate in the siRNA-containing media for 2 days for optimal knockdown. At 48 h post-treatment with siRNA, cells were inoculated with supernatants taken from HAstV-1-infected (MOI 10) Caco-2 cells in serum-free media for 1 h. Following virus adsorption, the inoculum was replaced with fresh media. At 24 hpi, cells were fixed in 100% methanol. Cells were washed in PBS and incubated in primary antibody solution containing astrovirus capsid monoclonal antibody 8e7 (Invitrogen MA5-16293) at 1:100 in 1% NGS/PBS for 1 h at room temperature. Cells were washed in PBS. Cells were incubated in secondary antibody solution containing Alexa Fluor 488 goat anti-Mouse (Invitrogen A10680) at 1:1,000 and and Hoechst (ThermoFisher H3569) at 1:2,000 in 1% NGS/PBS for 45 min in the dark. Cells were again washed in PBS. Samples were imaged using the EVOS FL cell imaging system and analyzed using ImageJ 2.9.0/1.53t software. FFU was calculated as previously described (45). The same method was used for supernatants from PIK-III- and DMSO-treated cell supernatants used to infect fresh Caco-2 cells in a 96-well plate.

Immunoblotting

Caco-2 cells were plated in a six-well plate (3.5×10^5). At 48 h post-plating, cells were inoculated with supernatants taken from HAstV-1 (MOI 10) or mock-inoculated Caco-2 cells in serum-free media for 1 h. Following virus adsorption, inoculum was

replaced with fresh media. At the proper time point, 8 or 24 hpi, cells were collected in 250 µL radioimmunoprecipitation assay (RIPA) lysis buffer (Abcam) containing 1× protease inhibitor cocktail (Pierce) on ice. Samples were vortexed briefly and kept on ice for 30 min. Samples were frozen at −80°C until used. Sample protein concentration was determined using BCA Protein Assay Kit (Pierce). Equal concentrations of protein were prepared under reducing conditions and separated by sodium dodecyl sulfate-polyacrylamide gel electrophoresis (4%–20% tris-glycine 1.0 mm Mini Protein Gels from Invitrogen XP04200BOX). Gels were transferred to polyvinylidene fluoride (PVDF) membranes using the iBlot 2 transfer stacks (ThermoFisher IB24002). Membranes were probed for protein with respective primary antibodies and IRDye 680RD goat anti-rabbit IgG secondary antibody using the ThermoFisher iBind device according to manufacturer's instructions. Primary antibodies included β-Actin (Cell Signaling 4970S) at 1:1,000, Atg5 (Abcam ab108327) at 1:1,000, and Atg7 (Abcam ab52472) at 1:1,000.

For siRNA experiments, Caco-2 cells were plated in a six-well plate (2.5×10^5). At 24 h post-plating, appropriate wells were treated with 15 µM siRNA (Atg5, Beclin, or Control siRNA). Cells were allowed to incubate in the siRNA-containing media for 2 days for optimal knockdown. At 48 h post-treatment with siRNA, cells were inoculated with supernatants taken from HAstV-1-infected (MOI 10) Caco-2 cells in serum-free media for 1 h. Following virus adsorption, the inoculum was replaced with fresh media. At 24 hpi, cells were collected in 250 µL RIPA lysis buffer (Abcam) containing 1× protease inhibitor cocktail (Pierce) on ice. Samples were vortexed briefly and kept on ice for 30 min. Samples were frozen at −80°C until used. Gels were run using the same protocol as above. Primary antibodies included β-Actin (Cell Signaling 4970S) at 1:1,000, Atg5 (Abcam ab108327) at 1:1,000, and Beclin (Abcam ab207612) at 1:1,000.

For Huh-7.5 immunoblots, Huh-7.5 cells were plated in a six-well plate (3×10^5). After 48 h, cells were treated with 1.5 µM or 6 µM doxycycline to induce RavZ protease activity or DMSO controls. At 24 h post-treatment, cells were inoculated with supernatants taken from HAstV-1-infected (MOI 10) Caco-2 cells in serum-free media for 1 h. Following virus adsorption, the inoculum was replaced with media containing the appropriate concentration of doxycycline or DMSO, as well as 30 µM chloroquine to enable monitoring of LC3-II/LC3-I (50). At 24 hpi, cells were collected in 250 µL RIPA lysis buffer (Abcam) containing 1× protease inhibitor cocktail (Pierce) on ice. Samples were vortexed briefly and kept on ice for 30 min. Samples were frozen at −80°C until used. Sample protein concentration was determined using BCA Protein Assay Kit (Pierce). Immunoblots were performed the same way as described with Caco-2 cell lysates. Membranes were probed for LC3 (Cell Signaling 2775S) at 1:1,000 overnight at 4°C in 5% BSA/Tris-buffered saline and Tween 20 (TBST). The following day, membranes were incubated in secondary antibody solution containing IRDye 680RD goat anti-rabbit IgG secondary antibody in 5% BSA/TBST for 1 h at room temperature. Membranes were imaged on the LI-COR Odyssey Fc (software version number 1.0.36). Next, membranes were stained for β-Actin (Cell Signaling 4970S) at 1:1,000 using the ThermoFisher iBind device as described above. All immunoblots were performed in triplicate. Each blot was imaged on the LI-COR Odyssey Fc. Densitometry was measured using Image Studio version 5.2 software.

PIK-III, siRNA, and astrovirus infection RT-PCR

For PIK-III experiments, Caco-2 cells were plated in a 96-well plate (2.5×10^4). At 48 h post-plating, cells were inoculated with supernatants taken from HAstV-1 (MOI 10) or mock-inoculated Caco-2 cells in serum-free media for 1 h. Following virus adsorption, the inoculum was replaced with fresh media or media containing 5, 10, or 25 µM PIK-III or DMSO control. At 24 hpi, supernatants were collected in TRIzol LS, cells were collected in TRIzol, and RNA was extracted per manufacturer's instructions. RNA was then utilized in RT-PCR to determine astrovirus genome copies, as previously described (46).

For siRNA experiments, Caco-2 cells were plated in a six-well plate (2.5×10^5). At 24 h post-plating, appropriate wells were treated with 15 µM siRNA (Atg5, Beclin, or Control siRNA). Cells were allowed to incubate in the siRNA-containing media for 2 days

for optimal knockdown. At 48 h post-treatment with siRNA, cells were inoculated with supernatants taken from HAstV-1-infected (MOI 10) Caco-2 cells in serum-free media for 1 h. Following virus adsorption, the inoculum was replaced with fresh media. At 24 hpi, cells were collected in TRIzol, and RNA was extracted per manufacturer's instructions. RNA was then utilized in RT-PCR to determine astrovirus genome copies, as previously described (46).

Huh-7.5 Rav-Z Induction

Huh-7.5 cells were plated in a six-well plate (3×10^5). After 48 h, cells were treated with 3 µM doxycycline to induce RavZ protease activity or DMSO control. At 24 h post-treatment, cells were inoculated with supernatants taken from HAstV-1-infected (MOI 10) Caco-2 cells in serum-free media for 1 h. Following virus adsorption, the inoculum was replaced with media containing the appropriate concentration of doxycycline or DMSO. At 24 hpi, supernatants were collected in TRIzol LS, and cells were collected in TRIzol. RNA was extracted from these samples according to the manufacturer's instructions. RNA was then utilized in RT-PCR to determine astrovirus genome copies, as previously described (46).

MuAstV 10× data set

The murine astrovirus 10× single-cell RNA sequencing data set was collected previously, as described (13).

Statistical analysis

Data were analyzed by two-way ANOVA followed by Tukey's multiple comparisons test (western blots, PIK-III genome copies, and PIK-III FFU analysis) or unpaired two-tailed *t*-test (Huh-7.5 cell genome copies and DMV electron microscopy quantification) to determine statistical significance using GraphPad Prism version 9. Asterisks show statistical significance as follows: *, $P \leq 0.05$; **, $P \leq 0.01$; ***, $P \leq 0.001$.

ACKNOWLEDGMENTS

Electron microscopy images were acquired with the help of Dr. Cam Robinson and Nathan Kurtz using the Electron Microscopy Shared Resource (SJCRH/ALSAC and NCI P30 CA021765). These studies were supported by an NIAID grant 1R03AI166434-01 and funding from ALSAC to S.S.C., K22 AI156116 to V.C., and NIAID grant R21 AI20113 to B.L.

AUTHOR AFFILIATIONS

[1]Department of Infectious Diseases, St. Jude Children's Research Hospital, Memphis, Tennessee, USA
[2]Integrated Program of Biomedical Sciences, Department of Microbiology, Immunology, and Biochemistry, University of Tennessee Health Science Center, Memphis, Tennessee, USA
[3]Graduate School of Biomedical Sciences, St. Jude Children's Research Hospital, Memphis, Tennessee, USA
[4]Department of Microbial Pathogenesis, Yale University, New Haven, Connecticut, USA
[5]Department of Comparative Medicine, Yale University, New Haven, Connecticut, USA
[6]Department of Molecular, Cellular, and Developmental Biology, University of California, Santa Cruz, California, USA
[7]Department of Immunology, St. Jude Children's Research Hospital, Memphis, Tennessee, USA

PRESENT ADDRESS

Virginia Hargest, Virginia Hargest, 3615 Civic Center Blvd, 503i, Philadelphia, Pennsylvania, USA

AUTHOR ORCIDs

Theresa Bub http://orcid.org/0000-0002-7330-9872
Stacey Schultz-Cherry http://orcid.org/0000-0002-2021-727X

FUNDING

Funder	Grant(s)	Author(s)
HHS | NIH | National Institute of Allergy and Infectious Diseases (NIAID)	1R03AI166434-01	Stacey Schultz-Cherry
American Lebanese Syrian Associated Charities (ALSAC)		Stacey Schultz-Cherry
HHS | NIH | National Institute of Allergy and Infectious Diseases (NIAID)	AI156116	Valerie Cortez

AUTHOR CONTRIBUTIONS

Theresa Bub, Conceptualization, Data curation, Formal analysis, Investigation, Methodology, Supervision, Writing – original draft, Writing – review and editing | Virginia Hargest, Data curation, Methodology, Writing – review and editing | Shaoyuan Tan, Formal analysis, Methodology, Writing – original draft, Writing – review and editing | Maria Smith, Data curation, Methodology, Writing – review and editing | Ana Vazquez-Pagan, Data curation, Methodology, Writing – review and editing | Tim Flerlage, Data curation, Methodology, Writing – review and editing | Pamela Brigleb, Methodology, Writing – review and editing | Victoria Meliopoulos, Methodology, Writing – review and editing | Brett Lindenbach, Methodology | Harish N. Ramanathan, Methodology, Resources | Valerie Cortez, Data curation, Writing – review and editing | Jeremy Chase Crawford, Data curation, Formal analysis, Methodology, Writing – review and editing | Stacey Schultz-Cherry, Conceptualization, Formal analysis, Funding acquisition, Investigation, Methodology, Project administration, Supervision, Writing – original draft, Writing – review and editing

DATA AVAILABILITY

The scRNA-seq data generated in this work is available at accession ID MK059949.1. Murine scRNA-seq can be accessed in NCBI BioProject with accession code PRJNA573959.

ADDITIONAL FILES

The following material is available online.

Supplemental Material

Figure S1 (JVI01025-23-s0001.tif). Supplemental figure.
Supplemental figure Legends (JVI01025-23-s0002.docx). Legends of Fig. S1 to S3.
Figure S2 (JVI01025-23-s0003.tif). Supplemental figure.
Figure S3 (JVI01025-23-s0004.tif). Supplemental figure.

REFERENCES

1. Bosch A, Pintó RM, Guix S. 2014. Human astroviruses. Clin Microbiol Rev 27:1048–1074. https://doi.org/10.1128/CMR.00013-14
2. Cortez V, Meliopoulos VA, Karlsson EA, Hargest V, Johnson C, Schultz-Cherry S. 2017. Astrovirus biology and pathogenesis. Annu Rev Virol 4:327–348. https://doi.org/10.1146/annurev-virology-101416-041742
3. Méndez E, Murillo A, Velázquez R, Burnham A, Arias CF. 2012. Replication cycle of astroviruses. Astrovirus Res:19–45. https://doi.org/10.1007/978-1-4614-4735-1
4. Moser L, Schultz-Cherry S. 2008. Astroviruses. Encycl Virol:204–210. https://doi.org/10.1016/B978-012374410-4.00348-4

5. Brinker JP, Blacklow NR, Herrmann JE. 2000. Human astrovirus isolation and propagation in multiple cell lines. Arch Virol 145:1847–1856. https://doi.org/10.1007/s007050070060
6. Guix S, Bosch A, Pintó RM. 2008. Astrovirus replication: an overview, p 571–595. In Structure-based study of viral replication. World Scientific. https://doi.org/10.1142/6324
7. Vu D-L, Bosch A, Pintó RM, Ribes E, Guix S. 2019. Human astrovirus MLB replication *in vitro*: persistence in extraintestinal cell lines. J Virol 93:e00557-19. https://doi.org/10.1128/JVI.00557-19
8. Hargest V, Davis AE, Tan S, Cortez V, Schultz-Cherry S. 2021. Human astroviruses: a tale of two strains. Viruses 13:376. https://doi.org/10.3390/v13030376
9. Koci MD, Moser LA, Kelley LA, Larsen D, Brown CC, Schultz-Cherry S. 2003. Astrovirus induces diarrhea in the absence of inflammation and cell death. J Virol 77:11798–11808. https://doi.org/10.1128/jvi.77.21.11798-11808.2003
10. Marvin SA. 2016. The immune response to astrovirus infection. Viruses 9:1. https://doi.org/10.3390/v9010001
11. Vu D-L, Cordey S, Brito F, Kaiser L. 2016. Novel human astroviruses: novel human diseases? J Clin Virol 82:56–63. https://doi.org/10.1016/j.jcv.2016.07.004
12. Vu D-L, Bosch A, Pintó RM, Guix S. 2017. Epidemiology of classic and novel human astrovirus: gastroenteritis and beyond. Viruses 9:33. https://doi.org/10.3390/v9020033
13. Cortez V, Boyd DF, Crawford JC, Sharp B, Livingston B, Rowe HM, Davis A, Alsallaq R, Robinson CG, Vogel P, Rosch JW, Margolis E, Thomas PG, Schultz-Cherry S. 2020. Astrovirus Infects actively secreting goblet cells and alters the gut mucus barrier. Nat Commun 11:2097. https://doi.org/10.1038/s41467-020-15999-y
14. Finkbeiner SR, Holtz LR, Jiang Y, Rajendran P, Franz CJ, Zhao G, Kang G, Wang D. 2009. Human stool contains a previously unrecognized diversity of novel astroviruses. Virol J 6:161. https://doi.org/10.1186/1743-422X-6-161
15. Blanchard E, Roingeard P. 2015. Virus-induced double-membrane vesicles. Cell Microbiol 17:45–50. https://doi.org/10.1111/cmi.12372
16. Hsu N-Y, Ilnytska O, Belov G, Santiana M, Chen Y-H, Takvorian PM, Pau C, van der Schaar H, Kaushik-Basu N, Balla T, Cameron CE, Ehrenfeld E, van Kuppeveld FJM, Altan-Bonnet N. 2010. Viral reorganization of the secretory pathway generates distinct organelles for RNA replication. Cell 141:799–811. https://doi.org/10.1016/j.cell.2010.03.050
17. Kirkegaard K, Taylor MP, Jackson WT. 2004. Cellular autophagy: surrender, avoidance and subversion by microorganisms. Nat Rev Microbiol 2:301–314. https://doi.org/10.1038/nrmicro865
18. Limpens R, van der Schaar HM, Kumar D, Koster AJ, Snijder EJ, van Kuppeveld FJM, Bárcena M. 2011. The transformation of enterovirus replication structures: a three-dimensional study of single- and double-membrane compartments. mBio 2:e00166-11. https://doi.org/10.1128/mBio.00166-11
19. Roingeard P, Eymieux S, Burlaud-Gaillard J, Hourioux C, Patient R, Blanchard E. 2022. The double-membrane vesicle (DMV): a virus-induced organelle dedicated to the replication of SARS-CoV-2 and other positive-sense single-stranded RNA viruses. Cell Mol Life Sci 79:425. https://doi.org/10.1007/s00018-022-04469-x
20. Suhy DA, Giddings TH, Kirkegaard K. 2000. Remodeling the endoplasmic reticulum by poliovirus infection and by individual viral proteins: an autophagy-like origin for virus-induced vesicles. J Virol 74:8953–8965. https://doi.org/10.1128/jvi.74.19.8953-8965.2000
21. Twu W-I, Lee J-Y, Kim H, Prasad V, Cerikan B, Haselmann U, Tabata K, Bartenschlager R. 2021. Contribution of autophagy machinery factors to HCV and SARS-CoV-2 replication organelle formation. Cell Rep 37:110049. https://doi.org/10.1016/j.celrep.2021.110049
22. Wolff G, Melia CE, Snijder EJ, Bárcena M. 2020. Double-membrane vesicles as platforms for viral replication. Trends Microbiol 28:1022–1033. https://doi.org/10.1016/j.tim.2020.05.009
23. Choi Y, Bowman JW, Jung JU. 2018. Autophagy during viral infection - a double-edged sword. Nat Rev Microbiol 16:341–354. https://doi.org/10.1038/s41579-018-0003-6
24. Kudchodkar SB, Levine B. 2009. Viruses and autophagy. Rev Med Virol 19:359–378. https://doi.org/10.1002/rmv.630
25. Mao J, Lin E, He L, Yu J, Tan P, Zhou Y. 2019. Autophagy and viral infection, p 55–78. In Autophagy regulation of innate immunity. https://doi.org/10.1007/978-981-15-0606-2
26. Stolz A, Ernst A, Dikic I. 2014. Cargo recognition and trafficking in selective autophagy. Nat Cell Biol 16:495–501. https://doi.org/10.1038/ncb2979
27. Codogno P, Mehrpour M, Proikas-Cezanne T. 2011. Canonical and non-canonical autophagy: variations on a common theme of self-eating?. Nat Rev Mol Cell Biol 13:7–12. https://doi.org/10.1038/nrm3249
28. Knoops KTB, Spiro A, de Groot L, Kromhout D, van Staveren WA, Tucker KL. 2009. Do dietary patterns in older men influence change in homocysteine through folate fortification? the normative aging study. Public Health Nutr 12:1760–1766. https://doi.org/10.1017/-S1368980008004321
29. Fahmy AM, Khabir M, Blanchet M, Labonté P. 2018. LC3B is not recruited along with the autophagy elongation complex (ATG5-12/16L1) at HCV replication site and is dispensable for viral replication. PLoS One 13:e0205189. https://doi.org/10.1371/journal.pone.0205189
30. Delorme-Axford E, Morosky S, Bomberger J, Stolz DB, Jackson WT, Coyne CB, Racaniello VR. 2014. BPIFB3 regulates autophagy and coxsackievirus B replication through a noncanonical pathway independent of the core initiation machinery. mBio 5:e02147. https://doi.org/10.1128/mBio.02147-14
31. Harris KG, Morosky SA, Drummond CG, Patel M, Kim C, Stolz DB, Bergelson JM, Cherry S, Coyne CB. 2015. RIP3 regulates autophagy and promotes coxsackievirus B3 infection of intestinal epithelial cells. Cell Host Microbe 18:221–232. https://doi.org/10.1016/j.chom.2015.07.007
32. Mohamud Y, Shi J, Tang H, Xiang P, Xue YC, Liu H, Ng CS, Luo H. 2020. Coxsackievirus infection induces a non-canonical autophagy independent of the ULK and PI3K complexes. Sci Rep 10:19068. https://doi.org/10.1038/s41598-020-76227-7
33. Gray EW, Angus KW, Snodgrass DR. 1980. Ultrastructure of the small intestine in astrovirus-infected lambs. J Gen Virol 49:71–82. https://doi.org/10.1099/0022-1317-49-1-71
34. Tange S, Zhou Y, Nagakui-Noguchi Y, Imai T, Nakanishi A. 2013. Initiation of human astrovirus type 1 infection was blocked by inhibitors of phosphoinositide 3-kinase. Virol J 10:153. https://doi.org/10.1186/1743-422X-10-153
35. Yu X, Long YC, Shen H-M. 2015. Differential regulatory functions of three classes of phosphatidylinositol and phosphoinositide 3-kinases in autophagy. Autophagy 11:1711–1728. https://doi.org/10.1080/15548627.2015.1043076
36. Choy A, Dancourt J, Mugo B, O'Connor TJ, Isberg RR, Melia TJ, Roy CR. 2012. The *Legionella* effector RavZ inhibits host autophagy through irreversible Atg8 deconjugation. Science 338:1072–1076. https://doi.org/10.1126/science.1227026
37. Sherwood RK, Roy CR. 2016. Autophagy evasion and endoplasmic reticulum subversion: the yin and yang of *Legionella* intracellular infection. Annu Rev Microbiol 70:413–433. https://doi.org/10.1146/annurev-micro-102215-095557
38. Lamb CA, Yoshimori T, Tooze SA. 2013. The autophagosome: origins unknown, biogenesis complex. Nat Rev Mol Cell Biol 14:759–774. https://doi.org/10.1038/nrm3696
39. Corona Velazquez AF, Jackson WT. 2018. So many roads: the multifaceted regulation of autophagy induction. Mol Cell Biol 38:e00303-18. https://doi.org/10.1128/MCB.00303-18
40. Oudshoorn D, Rijs K, Limpens R, Groen K, Koster AJ, Snijder EJ, Kikkert M, Bárcena M. 2017. Expression and cleavage of middle east respiratory syndrome Coronavirus nsp3–4 polyprotein induce the formation of double-membrane vesicles that mimic those associated with Coronaviral RNA replication. mBio 8:e01658-17. https://doi.org/10.1128/mBio.01658-17
41. Romero-Brey I, Merz A, Chiramel A, Lee J-Y, Chlanda P, Haselman U, Santarella-Mellwig R, Habermann A, Hoppe S, Kallis S, Walther P, Antony C, Krijnse-Locker J, Bartenschlager R. 2012. Three-dimensional architecture and biogenesis of membrane structures associated with hepatitis C virus replication. PLoS Pathog 8:e1003056. https://doi.org/10.1371/journal.ppat.1003056
42. Romero-Brey I, Berger C, Kallis S, Kolovou A, Paul D, Lohmann V, Bartenschlager R. 2015. NS5A domain 1 and polyprotein cleavage kinetics are critical for induction of double-membrane vesicles

associated with hepatitis C virus replication. mBio 6:e00759. https://doi.org/10.1128/mBio.00759-15
43. Guix S, Caballero S, Bosch A, Pintó RM. 2004. C-terminal nsP1a protein of human astrovirus colocalizes with the endoplasmic reticulum and viral RNA. J Virol 78:13627–13636. https://doi.org/10.1128/JVI.78.24.13627-13636.2004
44. Méndez E, Aguirre-Crespo G, Zavala G, Arias CF. 2007. Association of the astrovirus structural protein VP90 with membranes plays a role in virus morphogenesis. J Virol 81:10649–10658. https://doi.org/10.1128/JVI.00785-07
45. Marvin S, Meliopoulos V, Schultz-Cherry S. 2014. Human astrovirus propagation, purification and quantification. Bio-Protoc 4. https://doi.org/10.21769/BioProtoc.1078
46. Gu Z, Zhu H, Rodriguez A, Mhaissen M, Schultz-Cherry S, Adderson E, Hayden RT. 2015. Comparative evaluation of broad-panel PCR assays for the detection of gastrointestinal pathogens in pediatric oncology patients. J Mol Diagn 17:715–721. https://doi.org/10.1016/j.jmoldx.2015.06.003
47. Hargest V, Bub T, Neale G, Schultz-Cherry S. 2022. Astrovirus-induced epithelial-mesenchymal transition via activated TGF-β increases viral replication. PLoS Pathog 18:e1009716. https://doi.org/10.1371/journal.ppat.1009716
48. Cortez V, Livingston B, Sharp B, Hargest V, Papizan JB, Pedicino N, Lanning S, Jordan SV, Gulman J, Vogel P, DuBois RM, Crawford JC, Boyd DF, Pruett-Miller SM, Thomas PG, Schultz-Cherry S. 2023. Indoleamine 2,3-dioxygenase 1 regulates cell permissivity to astrovirus infection. Mucosal Immunol:S1933-0219(23)00042-9. https://doi.org/10.1016/j.mucimm.2023.05.011
49. Wu T, Hu E, Xu S, Chen M, Guo P, Dai Z, Feng T, Zhou L, Tang W, Zhan L, Fu X, Liu S, Bo X, Yu G. 2021. clusterProfiler 4.0: a universal enrichment tool for interpreting omics data. Innov Camb Mass2:100141. https://doi.org/10.1016/j.xinn.2021.100141
50. Klionsky DJ, Abdalla FC, Abeliovich H, Abraham RT, Acevedo-Arozena A, Adeli K, Agholme L, Agnello M, Agostinis P, Aguirre-Ghiso JA, Ahn HJ, Ait-Mohamed O, Ait-Si-Ali S, Akematsu T, Akira S, Al-Younes HM, Al-Zeer MA, Albert ML, Albin RL, Alegre-Abarrategui J, Aleo MF, Alirezaei M, Almasan A, Almonte-Becerril M, Amano A, Amaravadi RK, Amarnath S, Amer AO, Andrieu-Abadie N, Anantharam V, Ann DK, Anoopkumar-Dukie S, Aoki H, Apostolova N, Arancia G, Aris JP, Asanuma K, Asare NYO, Ashida H, Askanas V, Askew DS, Auberger P, Baba M, Backues SK, Baehrecke EH, Bahr BA, Bai X-Y, Bailly Y, Baiocchi R, Baldini G, et al. 2012. Guidelines for the use and interpretation of assays for monitoring Autophagy. Autophagy 8:445–544. https://doi.org/10.4161/auto.19496